Fast Port Selection using Temporal and Spatial Correlation for Fluid Antenna Systems

Shunhang Zhang, Jinghan Mao, Yanzhao Hou, Yu Chen, Kai-Kit Wong, and Xiaofeng Tao

***Abstract*—Fluid antenna system is a flexible antenna structure that obtains tremendous space diversity by allowing the antenna to change its position (or port) in a given space. The extraordinary performance requires the fluid antenna to always switch to the port with the largest signal-to-noise ratio (SNR) from a large number of ports. In practice, however, this means that a large number of channel observations (over all the ports) are required and the overhead could outweigh the benefits. In this paper, we exploit the spatial and temporal correlation of the channels in the fluid antenna ports using a machine learning approach. The proposed algorithm first estimates all the port channels in space from a small number of observations and then predicts the port channels in the subsequent time slots. Re-observations are used to reduce the error propagation in long short-term memory (LSTM) rolling window regression. Simulation results demonstrate that the proposed algorithm can achieve promising performance with few re-observations in high-mobility scenarios.**

***Index Terms*—Channel estimation, Fluid antenna system, Machine learning, Outage probability, Port selection, Prediction.**

I. Introduction

Multiple-input multiple-output (MIMO) antenna system has been the *de facto* technology in the physical layer of mobile communications for generations. It is blessed with rich literature of signal processing and coding schemes to obtain spatial diversity for reliability and/or capacity benefits [1]. While we have enjoyed huge success of MIMO and witnessed the rise of base station (BS) antennas to 64 in the fifth generation (5G) [2], [3], the same increase in the number of antennas from the mobile side is not seen due to space limitation. Moreover, note that MIMO also comes with considerable overhead in terms of channel estimation and complex optimization.

Recently, Wong *et al.* proposed an alternative method, which is referred to as fluid antenna system (FAS) [4], [5], to obtain the spatial diversity. FAS follows upon the recent advances in flexible antenna structures (e.g., liquid-based antennas [6]–[8] or reconfigurable pixel-based antennas [9]–[11]), to envisage that an antenna can change its position (referred to as 'port'), from a number of prescribed ports, on demand. In effect, the antenna would be able to scan through a 'continuous' fading envelope and access nearly any point in the given space. Early results in [4] indicated great potential in enhancing the outage probability performance and [12], [13] further looked into the capacity benefits of using FAS in multiuser environments.

The uplifting results seem to have motivated more research in FAS in recent years. For instance, Khammassi *et al.* improved the channel correlation model and used a covariance matrix approximation approach to analyze the outage probability for a single-user FAS [14]. Later in [15], the authors studied the performance enhancement of FAS in spatially correlated Nakagami fading channels. Unlike traditional systems, channel estimation in FAS is difficult, which was investigated in [16] where a linear minimum mean-square-error (LMMSE) channel estimation method was proposed in a multiuser setting. There was also the spin-off from FAS in [17] and [18] that advocated mobilization of antennas for diversity advantages. Instead of allowing the antenna(s) to move with high spatial resolution, however, they restrict the antenna(s) to only switch to a few uncorrelated ports, making it more like a MIMO with subgroup antenna selection. By contrast, a unique feature in FAS is that the ports are closely spaced and therefore their channels can be highly correlated. This characteristics enables FAS to avoid deep fade or interference even if space is at a premium.

Despite the optimism, one strong assumption in the previous works is that the FAS always selects the best port. For a user equipped with an N-port fluid antenna of size $W\lambda$ in which λ denotes the wavelength, the channel state information (CSI) at all N ports needs to be available at any given time in order to take full advantage of FAS. Note that N can be very large, say 100s. This would impose unbearable challenges for FAS. As the port channels are strongly correlated, deep learning can be useful in estimating the port CSI from knowing only a small subset of the ports. This was addressed for single-user systems in [19], [20] and multiuser systems in [21]. In this paper, we extend the work in [19], [20] to include temporal variation of the channels, and aim to develop a learning-based approach to not only estimate the port CSI in space but also predict the port CSI in subsequent time slots. One major difference from [19], [20] is that we employ the multi-ray channel model [22], [23] that can realistically model the correlation of FAS.

II. System Model

A. FAS

We consider a point-to-point communication system where the receiver is equipped with an N-port fluid antenna of length $W\lambda$. In this FAS, the antenna can be switched instantly to one of the N ports evenly distributed over its size. The received signal at the k-th port is given by

$$y_k = g_k x + \eta_k, \tag{1}$$

The work is supported in part by the Engineering and Physical Sciences Research Council (EPSRC) under Grant EP/W026813/1. For the purpose of open access, the authors will apply a Creative Commons Attribution (CC BY) licence to any Author Accepted Manuscript version arising.

S. Zhang, J. Mao, Y. Hou, Y. Chen, and X. Tao are with the School of Information and Communication Engineering (SICE), Beijing University of Posts and Telecommunications, China.

K. K. Wong is with the Department of Electronic and Electrical Engineering, University College London, Torrington Place, United Kingdom.

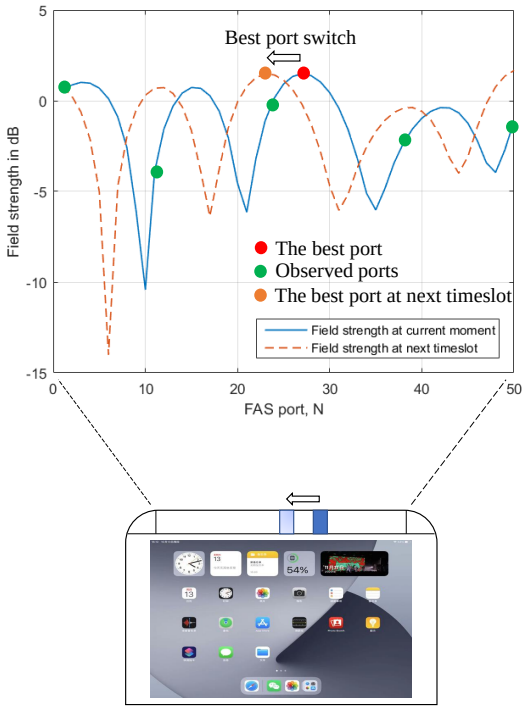

Fig. 1. Port selection of a FAS in time-varying environments.

where g_k is the complex channel coefficient at the k-th port, with $\mathrm{E}[|g_k|^2] = \Omega$, η_k represents the complex additive white Gaussian noise (AWGN) at the k-th port, with zero mean and variance of σ_η^2, and x denotes the information-bearing symbol. Note that the time index is omitted here but will be introduced back when temporal changes are discussed.

The average signal-to-noise ratio (SNR) at each port can be found as

$$\Gamma = \frac{\Omega \mathrm{E}\left[|x|^2\right]}{\sigma_\eta^2}. \tag{2}$$

B. Spatial and Temporal Correlation

We adopt a finite-scatterer channel model with azimuth and elevation angle-of-arrivals (AoAs) [22], [23]. Hence,

$$g_k = \sqrt{\frac{K\Omega}{K+1}} e^{j\alpha} \times e^{-j\frac{2\pi(k-1)W}{N-1}\sin\theta_0\cos\phi_0} + \sum_{l=1}^{N_p} a_l e^{-j\frac{2\pi(k-1)W}{N-1}\sin\theta_l\cos\phi_l} \tag{3}$$

in which K is the Rician factor, Ω is the total channel power, N_p is the number of scattered paths, α is the random phase shift of the specular component, θ_0 denotes the azimuth AoA of the specular component, ϕ_0 denotes the elevation AoA of the specular component, θ_l denotes the azimuth AoA of the l-th scattered path and ϕ_l denotes the elevation AoA of the l-th scattered path. Additionally, a_l represents a complex channel coefficient of the l-th scattered path, which we model as complex Gaussian. If N_p is large, then g_k will be complex Gaussian distributed. Since N can be very large, the ports can be arbitrarily close, so $\{g_k\}_{\forall k}$ is spatially correlated.

Now, assume that the receiver moves at a constant speed v. Then the CSI will change over time gradually as the channel paths combine slightly differently. With two-dimensional isotropic scattering and an isotropic receiver port, the autocorrelation function of the port channel satisfies [24]

$$\phi_{gg}(\tau) = \frac{\Omega}{2} J_0\left(2\pi f_m \tau\right) \tag{4}$$

where τ represents the time difference, and $f_m = v/\lambda$ is the maximum Doppler frequency. Introducing the time index t to the port channel in (3) to incorporate the temporal correlation, the channel at the k-th port at time t can be written as

$$g_{k,t} = \sqrt{\frac{K\Omega}{K+1}} e^{j\alpha} \times e^{-j\frac{2\pi(k-1)W}{N-1}\sin\theta_0\cos\phi_0} \times e^{-j\frac{2\pi vt}{\lambda}\sin\theta_0\cos\phi_0} + \sum_{l=1}^{N_p} a_l e^{-j\frac{2\pi(k-1)W}{N-1}\sin\theta_l\cos\phi_l} \times e^{-j\frac{2\pi vt}{\lambda}\sin\theta_l\cos\phi_l}. \tag{5}$$

C. SNR-Maximizing Port Selection

In order to achieve the best system performance, FAS needs to switch the radiating element to the port with the maximum SNR. Therefore, the optimal port is defined as

$$k_t^* = \arg\max\left\{|g_{1,t}|, |g_{2,t}|, \ldots, |g_{N,t}|\right\}, \tag{6}$$

where k_t^* denotes the index of the best port at time t. If we know all $|g_{k,t}|$, then it is easy to find k_t^*. However, in practical situations, the number of ports is large, N, and acquiring all the port CSI at all time slots is unviable.

According to [19], [20], it would be possible to acquire only about 30% of the port CSI in space and deep learning could be effective in estimating the remaining port CSI by exploiting the spatial correlation structure of the channels. Extending this approach to incorporate the temporal correlation as shown in Fig. 1, we have the estimated port CSI at time t as

$$\begin{aligned}\tilde{\boldsymbol{g}}_t &= [\tilde{g}_{1,t}\ \tilde{g}_{1,t}\ \cdots\ \tilde{g}_{N,t}] \\ &= f_1\left(\{\tilde{g}_{k,\nu}\}_{\forall k,\nu=t-L+1,\ldots,t-1}\right),\end{aligned} \tag{7}$$

in which the function f_1 may be derived using a deep learning approach, and the '$\sim$' notation specifies that the variables are estimated. Note that the port CSI at time t are assumed to be derived from previous port CSI up to the $(t-L+1)$-th time slot. As such, L represents the re-observation period. That is to say, for every L time slots, the port CSI will be estimated, not predicted. Evidently, only, say 30%, will be estimated.

For $t = 0, L, 2L, \ldots$, some port CSI is estimated and we denote the set containing the port indices of the estimated CSI as $\mathcal{K}$ while the set containing the port indices of the channels that are to be derived from the estimated ones is denoted by $\mathcal{U}$. Then the port CSI is obtained by

$$\tilde{\boldsymbol{g}}_t = f_2\left(\{g_{k,t}\}_{\forall k\in\mathcal{K}}\right), \text{ for } t = 0, L, 2L, \ldots, \tag{8}$$

where f_2 is the function that can be obtained using supervised learning as in [19], [20]. With $\tilde{\boldsymbol{g}}_t$, port selection of the FAS at time t can be found by

$$k_t^* = \arg\max_k \left[\tilde{\boldsymbol{g}}_t\right]_k. \tag{9}$$

TABLE I
LSTM NETWORK SETTING

Parameter	Value
Layer 1	50 LSTM cells (Bidirectional); input shape(1,N)
Layer 2	10 LSTM cells (Bidirectional)
Layer 3	50 Dense (Time distributed)
Batch size	128
Epochs	20
Optimizer	SGD with MSE as loss function
Learning rate	0.001

TABLE II
LSTM NETWORK SETTING

Parameter	Value
Layer 1	4 LSTM cells (Bidirectional); input shape(1,look-back)
Layer 2	10 LSTM cells (Bidirectional)
Layer 3	1 Dense
Batch size	32
Epochs	100
Optimizer	SGD with MSE as loss function
Learning rate	0.01

III. DEEP LEARNING PORT SELECTION

A. Estimation

Since temporal correlation exists, the channels at any given port over different time slots can be regarded as a time series. Similarly, the spatial correlation also means that the channels at different ports can be viewed as a time series. Long short-term memory (LSTM) is a temporal recurrent neural network (RNN) suitable for processing and predicting critical events with very long intervals and delays in time series [25]. It is generally better than RNN and hidden Markov model (HMM).

To exploit the spatial correlation between ports to solve (8), i.e., using $\{|g_k|\}_{k\in\mathcal{K}}$ to estimate $\{|g_k|\}_{k\in\mathcal{U}}$, we apply LSTM to treat the channel gains of the ports in space as a time series. Using supervised learning methods, LSTM models are trained with mean square error (MSE) as the loss function, i.e.,

$$\mathcal{L}_{\text{est}} = \mathrm{E}\left[\frac{1}{|\mathcal{U}|}\sum_{\ell\in\mathcal{U}}\left(|g_\ell| - |\tilde{g}_\ell|\right)^2\right], \tag{10}$$

where $\tilde{g}_\ell$ denotes the estimated value of the port channel output by the LSTM model, g_ℓ is the known true channel gain in the dataset. The parameters of the model are given in Table I.

B. Prediction

When using the LSTM network to predict the channels of the ports, the rolling window regression method is used with a step size of three. This means that the channels at time slot t are to be predicted using the knowledge of the channels from the previous 3 slots, i.e., $t-1, t-2, t-3$. As the sliding window regression method takes the previous predicted value as a new input each time, this can lead to an increasing error between the predicted value and the actual value. Therefore, a small number of ports are re-observed every L time slots to reduce the cumulative error. Again, using supervised learning, the LSTM model can be trained using the loss function

$$\mathcal{L}_{\text{pred}} = \mathrm{E}\left[\frac{1}{N|\mathcal{T}|}\sum_{k}\sum_{\nu\in\mathcal{T}}\left(|g_{k,\nu}| - |\tilde{g}_{k,\nu}|\right)^2\right], \tag{11}$$

where $\mathcal{T}$ include the present time index t and the 3 previous time indices $t-1, t-2, t-3$, $\tilde{g}_{k,t}$ is the output prediction of the LSTM model. The detailed parameters of this LSTM model are provided in Table II.

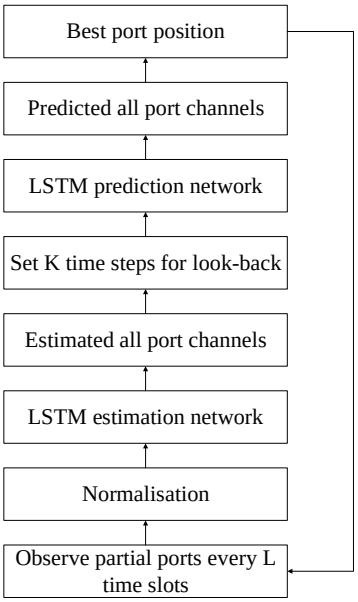

Fig. 2. The LSTM based port selection process.

C. Port Selection

The proposed LSTM based port selection process is given as a flowchart in Fig. 2. The process starts with pre-processing the input data. First of all, a small portion of the observed port channel data is normalized and imported into the LSTM estimation network to estimate the channels for all the ports. The normalized channel at the k-th port is given by

$$\hat{g}_k = \frac{g_k - \min\left(g_1, g_2, \ldots, g_N\right)}{\max\left(g_1, g_2, \ldots, g_N\right) - \min\left(g_1, g_2, \ldots, g_N\right)}, \tag{12}$$

where the time index is omitted.

Afterwards, set K time steps for look-back and import the estimated port channels into the LSTM prediction network to predict the port channels for the next time slot. Next the best port location is selected based on the predicted port channels and FAS switches the port to this location, completing the entire process of port selection using LSTM.

The time complexity of the scheme proposed in this paper is $O(|\mathcal{K}|t_0)$, which is greatly reduced compared to $O(|\mathcal{U}|T)$ of the original port selection scheme. Here, T represents all the time slots that need to be observed to achieve perfect system performance, while $t_0 = T/L$ represents the time slots that need to be observed for the proposed scheme.

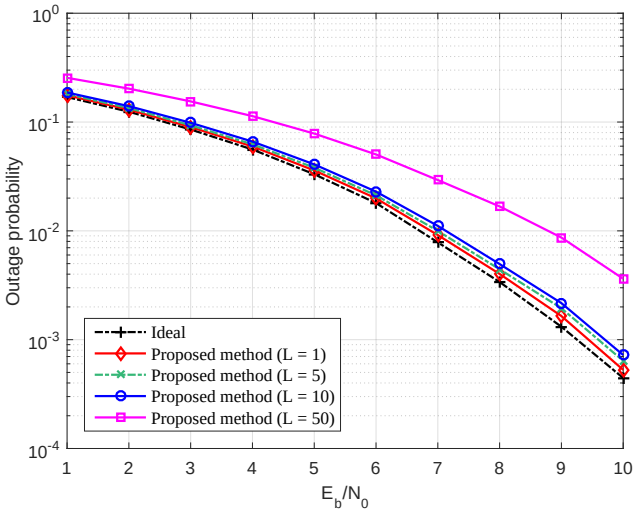

Fig. 3. Outage probability against the average SNR.

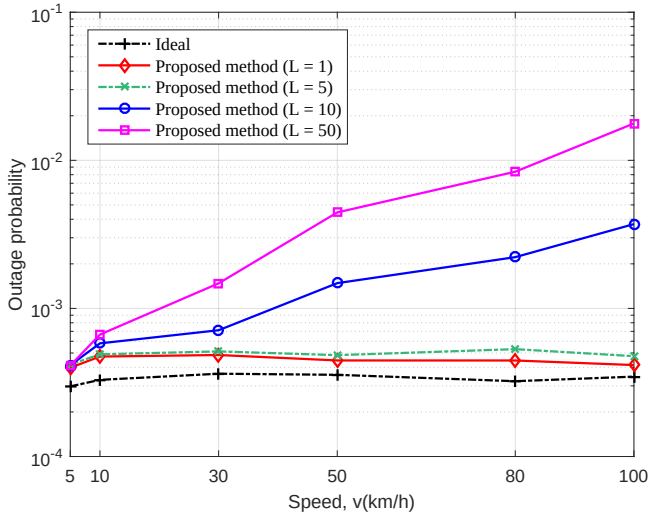

Fig. 4. Outage probability against the speed of the receiver.

IV. Simulation Results

In this section, we provide the simulation results to evaluate the proposed FAS port selection scheme. We consider $N = 20$, and 30% of the ports are observed through channel estimation. Under this setting, $|\mathcal{K}| = 6$, and the 1^{st}, 5^{th}, 9^{th}, 12^{th}, 16^{th} and 20^{th} ports are chosen as the observed (or known) ports. The wavelength λ is assumed to be 0.06m and a time slot is $66.67\mu s$ long. In addition, unless specified otherwise, the Rice factor K is 10, the normalized size W is 2 and $\Omega = 1$. In the simulation results, 'Ideal' corresponds to the FAS with perfect CSI while the results for the proposed method are given for different L where L specifies how often re-observation occurs. For example, if $L = 1$, then CSI re-observation takes place every time slot so CSI prediction only occurs in the spatial domain. The cases with $L = 5$ and $L = 10$ represent a more practical setup which observes the channels once every 5 or 10 time slots, respectively. Both significantly reduce the number of observations and enable fast FAS port selection with an acceptable loss of performance. In the extreme case of $L = 50$, the ports are only re-observed once every 50 time slots, which will keep CSI acquisition effort at minimum.

Fig. 3 provides the outage probability results of the proposed FAS for different L at various SNR. The speed of the receiver is set to $v = 30\text{km/h}$ and the number of scattered paths N_p is 5 (a typical rich scattering channel). As expected, the outage probability reduces as the SNR increases for all the methods considered. Moreover, the proposed FAS appears to achieve very nearly the performance of the ideal system even if L is as large as 10 although $L = 50$ is too large for CSI prediction. This indicates that the complexity of CSI estimation can be much reduced using the proposed method.

Fig. 4 examines the outage performance when the speed of the receiver changes at SNR of 10dB and with $N_p = 5$. Note that the ideal system performs nearly the same regardless of the speed, as expected. Also, the proposed FAS with $L \leq 5$ works really well even when the speed goes up to 100km/h. If $L = 10$, then the proposed FAS can cope with $v = 30\text{km/h}$ while $L = 50$ is even possible at $v = 10\text{km/h}$.

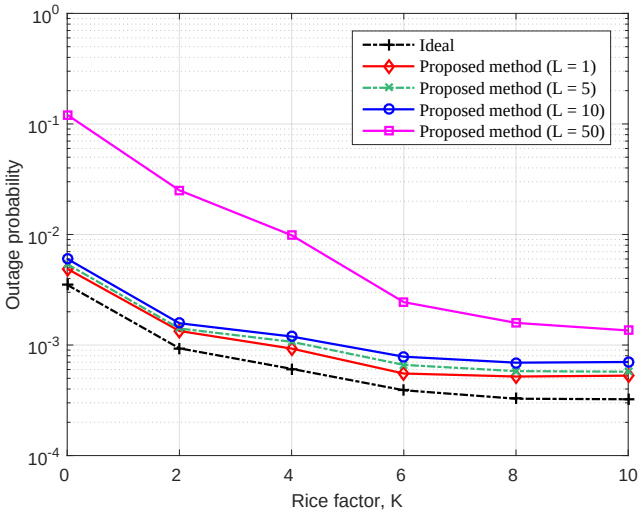

Fig. 5. Outage probability against the Rician factor of the channel.

Figs. 5 and 6 study how the outage performance varies if the channel parameters change assuming $v = 30\text{km/h}$ at SNR of 10dB. In Fig. 5, $N_p = 5$ when K is changed while for Fig. 6, $K = 10$ when N_p is varied. The results illustrate that generally speaking, when K or N_p increases, the outage probability of the systems improves. Another interesting observation is that as K or N_p increases, the importance of a small L appears to become less, as the performance gap between the ideal system and the proposed FAS with $L = 50$ reduces. In other words, if the channel either has a strong direct path or many scattered paths, then the proposed FAS with a large L is possible.

Lastly, Fig. 7 investigates the impact of the size of the fluid antenna for the proposed FAS when the average SNR is set to 10dB and $N_p = 5$. The results demonstrate that as W increases, the outage probability of the ideal system reduces, as expected. Nonetheless, the same trend is not observed for the proposed FAS. The reason is that when W increases, the correlation of the channels over the ports weakens, which will

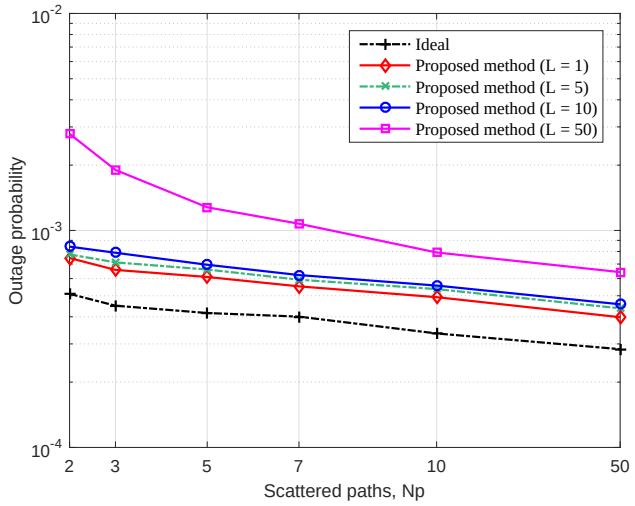

Fig. 6. Outage probability against the number of scattered paths.

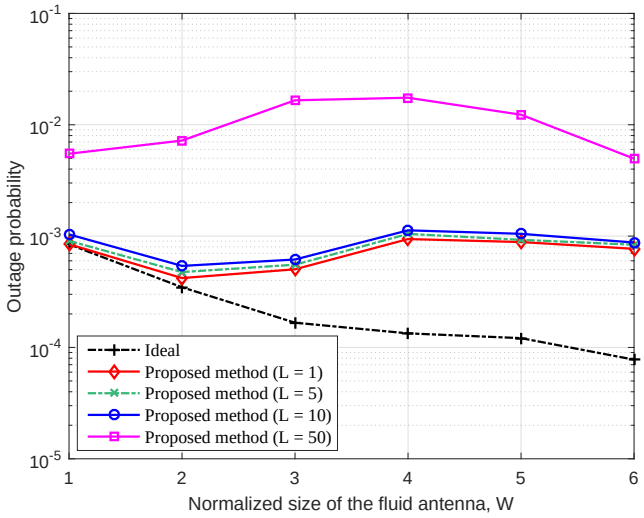

Fig. 7. Outage probability against the size of the fluid antenna, W.

make deep learning become less effective in estimation and prediction. That said, the performance of the proposed FAS still maintains at a good level. To improve the performance, one can consider increasing the number of port observations in space to improve the prediction performance.

V. Conclusion

This paper proposed an LSTM-based learning approach to estimate and predict the port CSI for fast port selection in a FAS by exploiting the spatial and temporal correlation of the channels. Simulation results demonstrated that the proposed approach could obtain decent outage probability performance in high mobility scenarios when only a small number of port CSI was observed, backing the feasibility of FAS.

References

[1] A. J. Paulraj, A. Gore, R. U. Nabar, and H. Bolcskei, "An overview of MIMO communications–A key to gigabit wireless," *Proc. IEEE*, vol. 92, no. 2, pp. 198–218, Feb. 2004.

[2] W. Hong *et al.*, "Multibeam antenna technologies for 5G wireless communications," *IEEE Trans. Antennas & Propag.*, vol. 65, no. 12, pp. 6231–6249, Dec. 2017.

[3] V. Jungnickel *et al.*, "The role of small cells, coordinated multipoint, and massive MIMO in 5G," *IEEE Commun. Mag.*, vol. 52, no. 5, pp. 44–51, May 2014.

[4] K. K. Wong, A. Shojaeifard, K. F. Tong, and Y. Zhang, "Fluid antenna systems," *IEEE Trans. Wireless Commun.*, vol. 20, no. 3, pp. 1950–1962, Mar. 2021.

[5] K. K. Wong, K. F. Tong, Y. Shen, Y. Chen, and Y. Zhang, "Bruce Lee-inspired fluid antenna system: Six research topics and the potentials for 6G," *Frontiers in Commun. and Netw., section Wireless Commun.*, 3:853416, Mar. 2022.

[6] Y. Huang, L. Xing, C. Song, S. Wang and F. Elhouni, "Liquid antennas: Past, present and future," *IEEE Open J. Antennas and Propag.*, vol. 2, pp. 473–487, 2021.

[7] X. Yan, L. Li, H. C. Zhang and J. Y. Han, "Broadband polarization-reconfigurable liquid dielectric resonator antenna controlled by gravity," *IEEE Antennas & Wireless Propag. Letters*, vol. 21, no. 10, pp. 2105–2109, Oct. 2022.

[8] X. Geng *et al.*, "Pattern-reconfigurable liquid metal magneto-electric dipole antenna," *IEEE Antennas & Wireless Propag. Letters*, vol. 21, no. 8, pp. 1683–1687, Aug. 2022.

[9] B. A. Cetiner, H. Jafarkhani, J.-Y. Qian, H. J. Yoo, A. Grau and F. De Flaviis, "Multifunctional reconfigurable MEMS integrated antennas for adaptive MIMO systems," *IEEE Commun. Mag.*, vol. 42, no. 12, pp. 62–70, Dec. 2004.

[10] A. Grau Besoli and F. De Flaviis, "A multifunctional reconfigurable pixeled antenna using MEMS technology on printed circuit board," *IEEE Trans. Antennas & Propag.*, vol. 59, no. 12, pp. 4413–4424, Dec. 2011.

[11] S. Song and R. D. Murch, "An efficient approach for optimizing frequency reconfigurable pixel antennas using genetic algorithms," *IEEE Trans. Antennas & Propag.*, vol. 62, no. 2, pp. 609–620, Feb. 2014.

[12] K. K. Wong, and K. F. Tong, "Fluid antenna multiple access," *IEEE Trans. Wireless Commun.*, vol. 21, no. 7, pp. 4801–4815, Jul. 2022.

[13] K. K. Wong, K. F. Tong, Y. Chen, and Y. Zhang, "Fast fluid antenna multiple access enabling massive connectivity," to appear in *IEEE Commun. Letters*, 2023.

[14] M. Khammassi, A. Kammoun, and M.-S. Alouini, "A new analytical approximation of the fluid antenna system channel," [Online] arXiv preprint arXiv:2203.09318, 2022.

[15] L. Tlebaldiyeva, G. Nauryzbayev, S. Arzykulov, A. Eltawil, and T. Tsiftsis, "Enhancing QoS through fluid antenna systems over correlated Nakagami-m fading channels," in Proc. *IEEE Wireless Commun. & Netw. Conf. (WCNC)*, pp. 78–83, 10-13 Apr. 2022, Austin, TX, USA.

[16] C. Skouroumounis and I. Krikidis, "Fluid antenna with linear MMSE channel estimation for large-scale cellular networks," to appear in *IEEE Trans. Commun.*, 2023.

[17] L. Zhu, W. Ma, and R. Zhang, "Modeling and performance analysis for movable antenna enabled wireless communications," [Online] arXiv preprint arXiv:2210.05325, 2022.

[18] W. Ma, L. Zhu, and R. Zhang, "MIMO capacity characterization for movable antenna systems," [Online] arXiv preprint arXiv:2210.05396, 2022.

[19] Z. Chai, K. K. Wong, K. F. Tong, Y. Chen, and Y. Zhang, "Port selection for fluid antenna systems," *IEEE Commun. Letters*, vol. 26, no. 5, pp. 1180–1184, May 2022.

[20] Z. Chai, K. K. Wong, K. F. Tong, Y. Chen, and Y. Zhang, "Performance of machine learning aided fluid antenna system with improved spatial correlation model," in Proc. *Int. Conf. 6G Netw. (6GNet)*, pp. 1–6, 6-8 Jul. 2022, Paris, France.

[21] N. Waqar, K. K. Wong, K. F. Tong, A. Sharples, and Y. Zhang, "Deep learning enabled slow fluid antenna multiple access," to appear in *IEEE Commun. Letters*, 2023.

[22] T. S. Rappaport, G. R. MacCartney, M. K. Samimi, and S. Sun, "Wideband millimeter-wave propagation measurements and channel models for future wireless communication system design," *IEEE Trans. Commun.*, vol. 63, no. 9, pp. 3029–3056, 2015.

[23] I. A. Hemadeh, K. Satyanarayana, M. El-Hajjar, and L. Hanzo, "Millimeter-wave communications: Physical channel models, design considerations, antenna constructions, and link-budget," *IEEE Commun. Surv. Tutor.*, vol. 20, no. 2, pp. 870–913, 2018.

[24] G. Stüber, *Principles of Mobile Communication*, Norwell, MA, USA: Kluwer, 2002.

[25] S. Hochreiter and J. Schmidhuber, "Long short-term memory," *Neural Computation*, vol. 9, no. 8, pp. 1735–1780, Dec. 1997.